Nondestructive evaluation of porosity content in the curved corner section of composite laminates using focused ultrasonic waves

AUTHOR(S):

Okahara, Takuma; Biwa, Shiro; Kuraishi, Akira

This manuscript has been published in:
Trans. ASME Journal of Nondestructive Evaluation, Diagnostics and Prognostics of Engineering Systems,
Vol. 1 (2018), 011009. DOI: 10.1115/1.4037546

Nondestructive evaluation of porosity content in the curved corner section of composite laminates using focused ultrasonic waves

Takuma Okahara

Department of Aeronautics and Astronautics, Graduate School of Engineering, Kyoto University, Katsura, Nishikyo-ku, Kyoto 615-8540, Japan

Shiro Biwa (corresponding author)

Department of Aeronautics and Astronautics, Graduate School of Engineering, Kyoto University, Katsura, Nishikyo-ku, Kyoto 615-8540, Japan

E-mail: biwa@kuaero.kyoto-u.ac.jp

Akira Kuraishi

Aerospace Company, Kawasaki Heavy Industries, Ltd., Kakamigahara, Gifu 504-8710, Japan

Abstract

The feasibility of utilizing focused ultrasonic waves for the nondestructive evaluation of porosity content in curved corner sections of carbon fiber reinforced plastic (CFRP) laminate structures is investigated numerically as well as experimentally. For this purpose, two-dimensional finite element simulations are carried out to clarify the wave propagation behavior and the reflection characteristics when the non-focused or focused ultrasonic wave impinges on the corner section of unidirectional and quasi-isotropic CFRP laminates from the inner side via water. The corresponding reflection measurements are carried out for the CFRP corner specimens in the pulse-echo mode using non-focusing, point-focusing and line-focusing transducers. The numerical simulations and the experiments show that the use of focused ultrasonic waves is effective in obtaining clearly distinguishable surface and bottom echoes from the curved corner section of CFRP laminates. The influence of the porosity content on the reflection waveforms obtained with different types of transducers is demonstrated experimentally. The experimental results indicate that the porosity content of the CFRP corner section can be evaluated based on the amplitude ratio of the surface and bottom echoes obtained with focusing transducers, if the calibration relation is appropriately established for different ply stacking sequences.

1. INTRODUCTION

Increased applications of carbon-fiber-reinforced plastics (CFRP) in aircraft structures highlight the importance of nondestructive testing to assure their structural integrity. Characterizing the porosity in CFRP laminates is one of the relevant topics since the presence of excess amount of minute pores can reduce the strength of the laminates. There have been numerous works on the evaluation of the porosity content in CFRP laminates based on the velocity and attenuation of ultrasonic waves [1-11]. More recently, the ultrasonic back-scattered waves from the interlaminar interfaces are also used to evaluate the porosity content [12-15]. Most of the foregoing works, however, have been carried out for plane CFRP laminates. Curved CFRP components are being increasingly used in aircraft structures, such as stringers and stiffeners on airframe skins. The complex geometry, the laminate structure and the material anisotropy of the curved CFRP components can not only lead to misorientation of ultrasonic beams, but also complicate the interpretation of acquired ultrasonic wave signals for porosity characterization.

The need to understand the wave propagation behavior in curved CFRP components highlights the role of computational approaches. There have already been some foregoing works on the computational modeling of ultrasonic wave propagation in CFRP components with complex geometries. Deydier et al. [16] studied the ultrasonic wave propagation in tapered CFRP laminates using a ray-theory method. Journiac et al. [17] followed a similar approach to analyze the ultrasonic wave transmission in a curved composite component. Dominguez et al. [18] numerically simulated the ultrasonic inspection of a composite radius part by a phased array transducer using the finite-difference time-domain (FDTD) technique. The flaw inspection results of a corner-shaped composite specimen by the phase array technique were reported by Xu and Zhou [19], who also showed the FDTD simulation of the ultrasonic flaw detection of an aluminum corner specimen by a phased array transducer.

Recently, Ito et al. [20] performed finite element simulations and measurements of the ultrasonic wave reflection at a curved corner section of the composite laminate structure. Their results indicate that the porosity in the corner section can be evaluated by the amplitude ratio of the surface and

bottom echoes of the laminate when it is probed from the outer side of the corner. On the other hand, the reflection waveforms become quite complex to interpret when the corner is probed from the inner side. In practical situations, however, the inspection from the inner side of the corner may be a preferable choice. In Ref. [20], the incidence of ultrasonic waves from a non-focusing transducer was considered. As a consequence, the use of focused ultrasonic waves still remains as a topic to be explored as it can be a potential solution to characterize the porosity in the corner section from the inner side.

It is thus the aim of this study to explore, numerically as well as experimentally, the feasibility of using focused ultrasonic waves for characterizing the porosity content in curved CFRP laminate structures. The numerical simulations and the experiments follow the approaches similar to those by Ito et al. [20] except that the present study considers the case where the corner section is probed from its inner side by the focused or non-focused ultrasonic wave. A special attention of this study is paid to the effectiveness of focused ultrasonic waves in obtaining clear echo signals which can be used for porosity characterization. Furthermore, the influence of the porosity content on the reflection waveform from the corner section of CFRP laminates is examined experimentally in order to investigate the possibility of ultrasonic evaluation of the porosity content.

2. NUMERICAL SIMULATIONS

2.1 Modeling

To clarify the effectiveness of focused ultrasonic waves in obtaining the reflection waveforms which can be used to evaluate the porosity content in the corner section, numerical simulations of the ultrasonic wave reflection at a curved corner section of CFRP laminate structure are carried out using the commercial finite element software MSC Marc. The two-dimensional numerical models shown in Fig. 1 are generated to simulate the incidence of the ultrasonic wave which is (a) non-focusing or (b) focusing to the corner section from the inner side and to analyze the subsequent reflection behavior. The water region is arranged in the inner side of the corner to simulate the local immersion measurement. The excitation boundary on the top of each model corresponds to the transducer element

surface which emits the ultrasound. The excitation boundary is a straight line in Fig. 1 (a) modeling a non-focusing transducer, and is a circular arc of radius 25 mm in Fig. 1 (b) modeling a focusing transducer. This radius of curvature is in accordance with the experiments to be described in Section 3 where focusing transducers of the nominal focal length of 1 inch are used. The excitation boundaries in Fig. 1 (a) and (b) both have the aperture angle of 29.4 deg and the width of 12.7 mm. As shown in Fig. 1 (b), the center of curvature of the arc of excitation boundary is at the mid-plane of the laminate.

The CFRP laminate modeled here consists of 16 unidirectional plies (total thickness 3 mm) and has a right-angle corner with the inner radius of curvature of 3 mm. Two types of stacking sequence are considered, namely, the unidirectional laminate $[0]_{16}$ and the quasi-isotropic laminate $[45/0/-45/90]_{2S}$. Each ply in the laminates is assumed to be a homogeneous orthotropic elastic solid. In Ref. [20], the elastic constants of the unidirectional laminate were determined experimentally based on the wave velocities in different propagation directions measured by the double through-transmission technique [21], and used as the elastic constants of each ply. When the x axis is taken along the ply thickness direction and the y axis along the fiber direction, the assumed stress-strain relation of each ply is given by

$$\begin{pmatrix} \sigma_x \\ \sigma_y \\ \sigma_z \\ \tau_{yz} \\ \tau_{zx} \\ \tau_{xy} \end{pmatrix} = \begin{bmatrix} 13.4 & 6.84 & 7.00 & 0 & 0 & 0 \\ 6.84 & 120 & 7.65 & 0 & 0 & 0 \\ 7.00 & 7.65 & 13.5 & 0 & 0 & 0 \\ 0 & 0 & 0 & 4.88 & 0 & 0 \\ 0 & 0 & 0 & 0 & 3.11 & 0 \\ 0 & 0 & 0 & 0 & 0 & 4.99 \end{bmatrix} \begin{pmatrix} \varepsilon_x \\ \varepsilon_y \\ \varepsilon_z \\ \gamma_{yz} \\ \gamma_{zx} \\ \gamma_{xy} \end{pmatrix}, \tag{1}$$

where the numerical values for the elastic constants are in GPa. The same elastic constants and the density (1.54×10^3 kg/m^3) are also employed in the present analysis. The stiffness property of each point in the curved laminate structure is determined by carrying out appropriate transformations of the stiffness components accounting for the stacking direction of each ply and the curvature of the structure. Although thin resin layers between the plies have some significant effects on the wave propagation behavior at higher frequencies around the stop band of the layered structure [22, 23], such effects are ignored in the present simulations as the frequency range of the present interest is

sufficiently low. Consequently, the plies are assumed to be perfectly bonded to each other without the resin layers in this analysis. The numerical model region (CFRP structure and water) is discretized using four-node and three-node isoparametric elements, the total number of elements being 1,077,323 for Fig. 1 (a) and 1,091,932 for Fig. 1 (b).

2.2 Analysis of the Wave Field and the Reflection Waveform

In accordance with the experiments described later, the incidence of the longitudinal wave packet of the center frequency of 2.25 MHz is numerically simulated by prescribing the uniform distribution of the normal stress σ on the excitation boundary as a function of time t as

$$\sigma(t) = \sigma_0 \exp\left\{-\frac{(t-t_0)^2}{\tau_0^{\,2}}\right\}\cos\{2\pi f_0(t-t_0)\}, \tag{2}$$

where f_0 = 2.25 MHz, t_0 = 1 μs and τ_0 = 0.32 μs. The amplitude parameter σ_0 is chosen arbitrarily as unity due to the linear nature of the problem. The other boundaries of the numerical model are assumed to be traction-free except that the edges of the CFRP structure are fixed. The time evolution of the wave field is computed in an implicit manner using the Newmark-β method with the time step of 10 ns.

To obtain the reflection waveform corresponding to the pulse-echo measurement, the time history of the particle velocity in the sound-axis direction is spatially averaged on the excitation boundary. This waveform contains the excitation signal corresponding to Eq. (2) as well as the reflection signal from the CFRP structure. The half of the maximum peak-to-peak height of the excitation signal is regarded as the amplitude of the incident wave, and used to normalize the reflection waveform.

2.3 Numerical Results

Figure 2 shows the distributions of the particle velocity magnitude at different elapsed times for (a) the unidirectional and (b) the quasi-isotropic laminate structures, each for the cases of non-focusing as well as focusing of the incident wave. Due to the symmetry of the problem, only the left or the right half of the model is shown. In Fig. 2 (a) and (b), the non-focused incident wave first reaches the plane

surface of the structure. The wave refracted there then propagates within the laminate towards the corner, and interferes with the main wave which propagates along the beam axis and hits the corner directly from the water. As a result, the reflected wave is a superposition of the signals which have traveled different paths in the structure. On the other hand, the focused incident wave insonifies the corner section dominantly. As a consequence, the reflected wave in this case is expected to bear the information of material properties of the local region of the corner in a more straightforward manner.

The computed reflection waveforms are shown in Fig. 3 for both types of laminates. In Fig. 3 (a) for the unidirectional laminate, it is shown that the focused incident wave enhances the magnitudes of the surface and bottom echoes from the laminate, and is expected to facilitate their discrimination. In Fig. 3 (b) for the quasi-isotropic laminate, the surface and bottom echoes cannot be distinguished in the waveform for the non-focused incident wave, while they can be discriminated clearly for the focused incident wave. Namely, the present numerical simulations indicate that the surface and bottom echoes can be identified in the reflection waveform from the corner section obtained by probing it from the inner side by the focused ultrasonic wave.

The numerical results also show that the bottom echo is higher than the surface echo in Fig. 3 (b) for the quasi-isotropic laminate, while the former is weaker than the latter in Fig. 3 (a) for the unidirectional laminate. This is attributed to the difference in the in-plane elastic properties of both laminates. The more enhanced bottom echo for the quasi-isotropic laminate is also apparent in Fig. 2 (b). Namely, in the wave field at the elapsed time of 30 μs, the second wave front propagating upwards corresponding to the bottom echo is more salient than the surface echo.

3. EXPERIMENTS

3.1 Specimens

Based on the findings from the numerical simulations, the experiments are carried out to confirm the feasibility of focused ultrasonic waves to obtain clear reflection waveforms from the CFRP corner section and to investigate the influence of porosity on them. The CFRP corner specimens of the unidirectional and quasi-isotropic stacking sequences ($[0]_{16}$ and $[45/0/-45/90]_{2S}$) used here are the

same as those used in the previous study [20] which were fabricated using the Toho Tenax UTS50/135 UD prepreg. The dimensions of the corner specimens are schematically shown in Fig. 4. The specimens have the thickness of 3 mm and the right-angle corner section of inner radius of curvature of 3 mm. In addition to the porosity-free specimens manufactured with the regular procedures, porosity-containing specimens manufactured by irregular procedures were also used. The porosity of each specimen was evaluated by quantifying the area ratio of pores in the micrographs of the edge faces. The evaluated values of porosity were 3.7 % and 4.3 % for the unidirectional laminates and 1.6 % and 4.0 % for the quasi-isotropic laminates [20].

3.2 Local Immersion Measurement

The corner specimen was fixed on an acrylic holder by water-proof tapes and immersed in a water bath while retaining an air volume under the corner section as shown in Fig. 5, thereby achieving the local immersion measurement using an ordinary ultrasonic imaging system (Flex-Scan by Insight Co. Ltd., Japan). Three kinds of Panametrics piezoelectric transducers, i.e., non-focusing, line-focusing and point-focusing types, were used as an emitter as well as a receiver of the ultrasonic wave signal. The three transducers have the same nominal element diameter of 0.5 inch and the same nominal center frequency of 2.25 MHz. The nominal focal lengths of the point-focusing and line-focusing transducers are both 1 inch. When the focusing transducers were used, the distance of the transducer element to the corner surface was first set to around 25 mm, and adjusted to the position where the surface echo amplitude was maximal. The orientation of the focus line of the line-focusing transducer was arranged parallel with the longitudinal direction of the corner specimen (perpendicular to the plane of the cross-section shown in Fig. 5). The distance to the specimen was also set to be about 25 mm for the non-focusing transducer.

In the measurement, the transducer was excited by a spike voltage signal using a Panametrics 5072PR pulser-receiver to send a longitudinal wave pulse toward the corner section via water. The reflected wave was recorded by the same transducer in the pulse-echo mode. A hundred synchronized waveforms were averaged in a digital oscilloscope to enhance the signal-to-noise ratio and stored in a

personal computer as the reflection waveform.

4. EXPERIMENTAL RESULTS AND DISCUSSION

4.1 Reflection Waveforms of Porosity-Free Specimens

Figure 6 shows the recorded reflection waveforms of the porosity-free specimens of (a) the unidirectional and (b) the quasi-isotropic laminates, when probed using the non-focusing, point-focusing and line-focusing transducers. The locations of the reflection signals by the non-focusing transducer have some shifts from those by the focusing transducers, most likely due to the concave surfaces of the focusing transducers which have slightly longer effective propagation distances. It is clearly shown in Fig. 6 (a) and (b) that the waveforms of the focusing transducers have clearer surface and bottom echoes than those of the non-focusing transducer. The use of the non-focusing transducer resulted in weaker signals for both laminates, and makes the distinction between the surface and bottom echoes difficult in the waveform for the quasi-isotropic laminate. These features qualitatively verify the findings obtained by the numerical simulations. Namely, it has been shown both numerically and experimentally that the use of focused ultrasonic wave is effective in clearly discriminating the surface and bottom echoes of the corner section for both types of stacking sequence.

Between the point- and line-focusing transducers, it appears in Fig. 6 that the latter is slightly more advantageous in obtaining clearer bottom echoes. This is likely the outcome of the two-dimensional nature of focusing of the line-focusing transducer as compared to the three-dimensional focusing of the point-focusing transducer. In the results obtained by the line-focusing transducer, the bottom echo is more enhanced for the quasi-isotropic laminate than for the unidirectional laminate, in qualitative agreement with the observation made in Section 2.3 by means of the two-dimensional numerical simulations.

4.2 Influence of Porosity on the Reflection Waveform

The recorded reflection waveforms of (a) the unidirectional and (b) the quasi-isotropic laminates

with different porosity contents are shown in Figs. 7 to 9 when measured with the non-focusing, point-focusing and line-focusing transducers, respectively. It is first seen in Fig. 7 that only weak reflection signals are obtained with the use of the non-focusing transducer. For the unidirectional laminates, the bottom echoes are even less clear for the porosity-containing specimens. For the quasi-isotropic laminates, the waveform involves complicated echoes even in the absence of porosity as discussed above, and this complexity still persists when the porosity content increases. As a consequence, the porosity characterization based on these waveforms appears to be a difficult task.

In Fig. 8 for the point-focusing transducer, the bottom echo becomes weaker as the porosity content increases for both laminates, indicating the effect of wave attenuation due to the scattering by the pores. It is also noted that for high porosity contents, the surface echo is also changed in its shape, which is a feature not apparent in the waveforms in Fig. 7 or in the results of the previous study [20] obtained by non-focusing transducers. Similar trends are observed in Fig. 9 for the line-focusing transducer, with the shape change in the surface echo being more significant. This indicates that the reflection waveform is more sensitive to the inhomogeneous structure of the inspected material when focused waves are used.

4.3 Relation between the Amplitude Ratio and the Porosity Content

The attenuation of ultrasonic waves is commonly used as a measure to characterize the porosity content in composite laminates [4-9]. For plane plate specimens, the quantitative evaluation of attenuation coefficient is possible by the calibration accounting for the ultrasonic beam diffraction and the insertion loss due to the difference of acoustic impedances between the laminate and the coupling medium, e.g. [24]. For curved laminates considered here, however, such procedures are not straightforward, and therefore a simplistic approach is chosen. Namely, the amplitude ratio of the surface and bottom echoes in the reflection waveform is examined as a measure of ultrasonic wave attenuation. From the reflection waveforms measured on five different locations along the longitudinal direction of each corner specimen, the ratios of the maximum peak-to-peak height of the surface and bottom echoes were calculated. These ratios are plotted in Fig. 10 against the porosity content for (a)

the unidirectional and (b) the quasi-isotropic laminates using two kinds of focusing transducers. In Fig. 10 (a) and (b), the amplitude ratios show the decreasing trend with the porosity content, indicating that the porosity-content estimation is possible based on these relations. It should be noted here that the porosity contents in Fig. 10 were measured on the edge faces of the specimens and do not represent the local porosity contents corresponding to the waveform measurements: plotting the amplitude ratios against the local porosity contents could improve the correlation quantitatively.

In the previous study [20], it was demonstrated with the use of a non-focusing transducer that the amplitude ratio decreases with the porosity content when the corner section is probed from the outer side. In this case, the effect of ply stacking sequences on the relation between the amplitude ratio and the porosity content was found to be insignificant. In the present experiment, however, the quasi-isotropic laminates show higher amplitude ratios than the unidirectional laminates. Furthermore, the relation between the amplitude ratio and the porosity content also depends on the type of the transducer. Namely, the line-focusing transducer gives higher amplitude ratios than the point-focusing transducer. These features have an important implication for the practical applications, since different correlation curves should be established for estimating the porosity content by the amplitude ratio for different types of ply stacking sequences and for different types of transducers used.

5. CONCLUSION

The reflection behavior of focused ultrasonic waves at a curved corner section of CFRP laminate structure has been investigated based on the two-dimensional finite element simulations and the corresponding experiments. In particular, the reflection waveforms have been compared between the cases when non-focused and focused waves are used to probe the corner section from the inner side via water. The numerical simulations and the experiments have shown that the use of focused ultrasonic waves is effective in obtaining clearly distinguishable surface and bottom echoes for the curved corner section of unidirectional as well as quasi-isotropic CFRP laminates. The influence of porosity on the reflection waveform from the corner section has been demonstrated experimentally when non-focusing as well as focusing transducers are used. The experimental results indicate that the

porosity content of the CFRP corner section can be evaluated based on the amplitude ratio of the surface and bottom echoes obtained with focusing transducers, if the calibration relation is appropriately established for different ply stacking sequences and geometries. Although the experimental results have been obtained in this study with single focusing transducers, the wave focusing can be similarly achieved by using phased array transducers. The finite element simulations presented here are expected to serve as a useful tool to design an appropriate focusing method to obtain clear ultrasonic signals for the characterization of porosity in curved CFRP components and other practical geometries.

ACKNIOWLEDGMENT

The authors thank Mr. Michio Ohno, Kawaju Gifu Engineering Co., for his contribution in manufacturing the specimens with controlled porosity levels.

REFERENCES

[1] Reynolds, W. N., and Wilkinson, S. J., 1978, “The Analysis of Fibre-Reinforced Porous Composite Materials by the Measurement of Ultrasonic Wave Velocities,” Ultrasonics, **16**, pp. 159–163.

[2] Hsu, K. and Jeong, H., 1989, “Ultrasonic Velocity Change and Dispersion due to Porosity in Composite Laminates,” Review of Progress in Quantitative Nondestructive Evaluation, **8B**, pp. 1567–1573.

[3] Komsly, I. N., Daniel, I. M. and Wooh, S. C., 1993, “Characterization of Porosity in Thick Composites Using Ultrasonic Wave Velocity Measurements,” Review of Progress in Quantitative Nondestructive Evaluation, **12A**, pp. 1273–1280.

[4] Stone, D. E. W. and Clarke, B., 1975, “Ultrasonic Attenuation as a Measure of Void Content in Carbon Fibre Reinforced Plastics,” Non-Destructive Testing, **8**, p. 137-145.

[5] Hale, J. M. and Ashton, J. N., 1988, “Ultrasonic Attenuation in Voided Fibre-Reinforced Plastics,” NDT Int., **21**, p. 321-326.

[6] Daniel, I. M., Wooh, S. C. and Komsky, I., 1992, “Quantitative Porosity Characterization of

Composite Materials by Means of Ultrasonic Attenuation Measurements," J. Nondestruct. Eval., **11**, pp. 1-8.

[7] Guo, N. and Cawley, P., 1994, "The Non-Destructive Assessment of Porosity in Composite Repairs," Composites, **25**, pp. 842-850.

[8] Jeong, H., 1997, "Effects of Voids on the Mechanical Strength and Ultrasonic Attenuation of Laminated Composites," J. Compos. Mater., **31**, pp. 276-292.

[9] Birt, E. A. and Smith, R. A., 2004, "A Review of NDE Methods for Porosity Measurement in Fibre-Reinforced Polymer Composites," Insight, **46**, pp. 681-686.

[10] Park, J.-W., Kim, D.-J., Im, K.-H., Park, S.-K., Hsu, D. K., Kite, A. H., Kim, S.-K., Lee, K.S. and Yang, I.-Y., 2008, "Ultrasonic Influence of Porosity Level on CFRP Composite Laminates Using Rayleigh Probe Waves," Acta Mech. Solida Sinica, **21**, pp. 298-307.

[11] Lin, L., Zhang, X., Chen, J., Mu, Y. and Li, X., 2011, "A Novel Random Void Model and Its Application in Predicting Void Content of Composites Based on Ultrasonic Attenuation Coefficient," Appl. Phys. A, **103**, pp. 1153-1157.

[12] Dominguez, N. and Mascaro, B., 2006, "Ultrasonic Non-Destructive Inspection of Localized Porosity in Composite Materials," Proceedings of the 9th European Conference on Non-Destructive Testing 2006, Tu.2.1.4.

[13] Grolemund, D. and Tsai, C., 1998, "Statistical Moments of Backscattered Ultrasound in Porous Fiber Reinforced Composites," IEEE Trans. Ultrason. Ferroelectr. Freq. Control, **45**, pp. 295–304.

[14] Kim, K. B., Hsu, D. K. and Barnard, D. J., 2013, "Estimation of Porosity Content of Composite Materials by Applying Discrete Wavelet Transform to Ultrasonic Backscattered Signal," NDT & E Int., **56**, pp. 10–16.

[15] Ishii, Y., Biwa, S. and Kuraishi, A., 2016, "Influence of Porosity on Ultrasonic Wave Velocity, Attenuation and Interlaminar Interface Echoes in Composite Laminates: Finite Element Simulations and Measurements," Compos. Struct., **152**, pp. 645-653.

[16] Deydier, S., Gengembre, N., Calmon, P., Mengeling, V. and Pétillon, O., 2005, "Ultrasonic Field

Computation into Multilayered Composite Materials Using a Homogenization Method Based on Ray Theory," AIP Conf. Proc., **760**, pp. 1057-1064.

[17] Journiac, S., Leymarie, N., Dominguez, N. and Potel, C., 2011, "Simulation of Ultrasonic Inspection of Composite Using Bulk Waves: Application to Curved Components," J. Phys. Conf. Series, **269**, 012022.

[18] Dominguez, N., Grellou, O. and Van-der-Veen, S., 2010, "Simulation of Ultrasonic NDT in Composite Radius," 10th European Conference on Non-Destructive Testing (Moscow, June 2010), 1-10-41.

[19] Xu, N. and Zhou, Z., 2014, "Numerical Simulation and Experiment for Inspection of Corner-Shaped Components Using Ultrasonic Phased Array," NDT & E Int., **63**, pp. 28-34.

[20] Ito, J., Biwa, S., Hayashi, T. and Kuraishi, A., 2015, "Ultrasonic Wave Propagation in the Corner Section of Composite Laminate Structure: Numerical Simulations and Experiments," Compos. Struct., **123**, pp. 78-87.

[21] Rokhlin, S. I. and Wang, W., 1992, "Double Through-Transmission Bulk Wave Method for Ultrasonic Phase Velocity Measurement and Determination of Elastic Constants of Composite Materials," J. Acoust. Soc. Am., **91**, pp. 3303-3312.

[22] Ishii, Y. and Biwa, S., 2015, "Transmission of Ultrasonic Waves at Oblique Incidence to Composite Laminates with Spring-Type Interlayer Interfaces," J. Acoust. Soc. Am., **138**, pp. 2800-2810.

[23] Ishii, Y. and Biwa, S., 2017, "Ultrasonic Wave Transmission and Bandgap in Multidirectional Composite Laminates with Spring-Type Interlayer Interfaces," J. Acoust. Soc. Am., **141**, pp. 1099-1110.

[24] Wu, P. and Stepinski, T., "Quantitative Estimation of Ultrasonic Attenuation in a Solid in the Immersion Case with Correction of Diffraction Effects," Ultrasonics, **38**, pp. 481-485.

FIGURE CAPTIONS

Fig. 1 Finite element model for a corner section of CFRP laminate in the case of (a) non-focusing and (b) focusing of ultrasonic waves

Fig. 2 Snapshots of wave propagation in the case of non-focusing and focusing of incident waves for (a) unidirectional and (b) quasi-isotropic laminates

Fig. 3 Computed reflection waveforms in the case of non-focusing and focusing of incident waves for (a) unidirectional and (b) quasi-isotropic laminates

Fig. 4 Dimensions of the CFRP corner specimen

Fig. 5 Schematic illustration of the specimen arrangement in the reflection measurement

Fig. 6 Measured reflection waveforms obtained with non-focusing and focusing transducers for (a) unidirectional and (b) quasi-isotropic laminates

Fig. 7 Measured reflection waveforms obtained with the non-focusing transducer for (a) unidirectional and (b) quasi-isotropic laminates with different porosity contents

Fig. 8 Measured reflection waveforms obtained with the point-focusing transducer for (a) unidirectional and (b) quasi-isotropic laminates with different porosity contents

Fig. 9 Measured reflection waveforms obtained with the line-focusing transducer for (a) unidirectional and (b) quasi-isotropic laminates with different porosity contents

Fig. 10 Amplitude ratio of surface and bottom echoes with respect to the porosity content for (a) unidirectional and (b) quasi-isotropic laminates

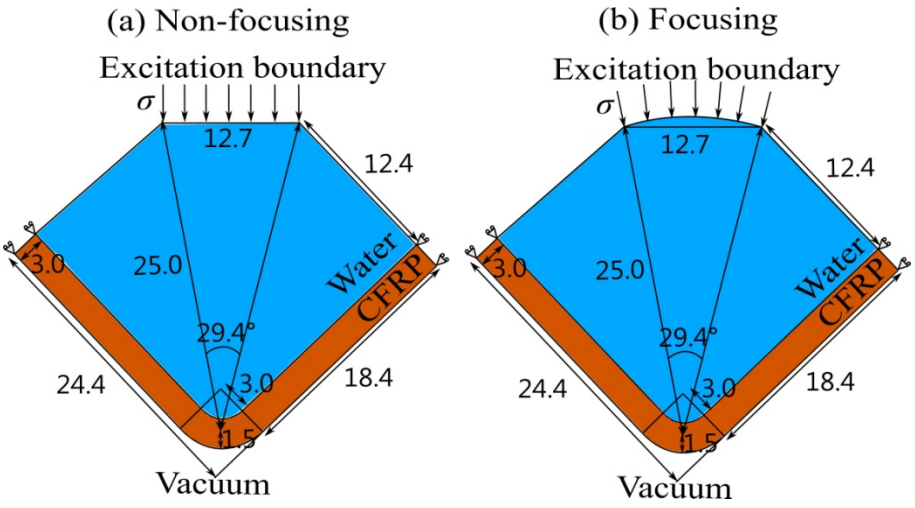

Fig. 1 Finite element model for a corner section of CFRP laminate in the case of (a) non-focusing and (b) focusing of ultrasonic waves

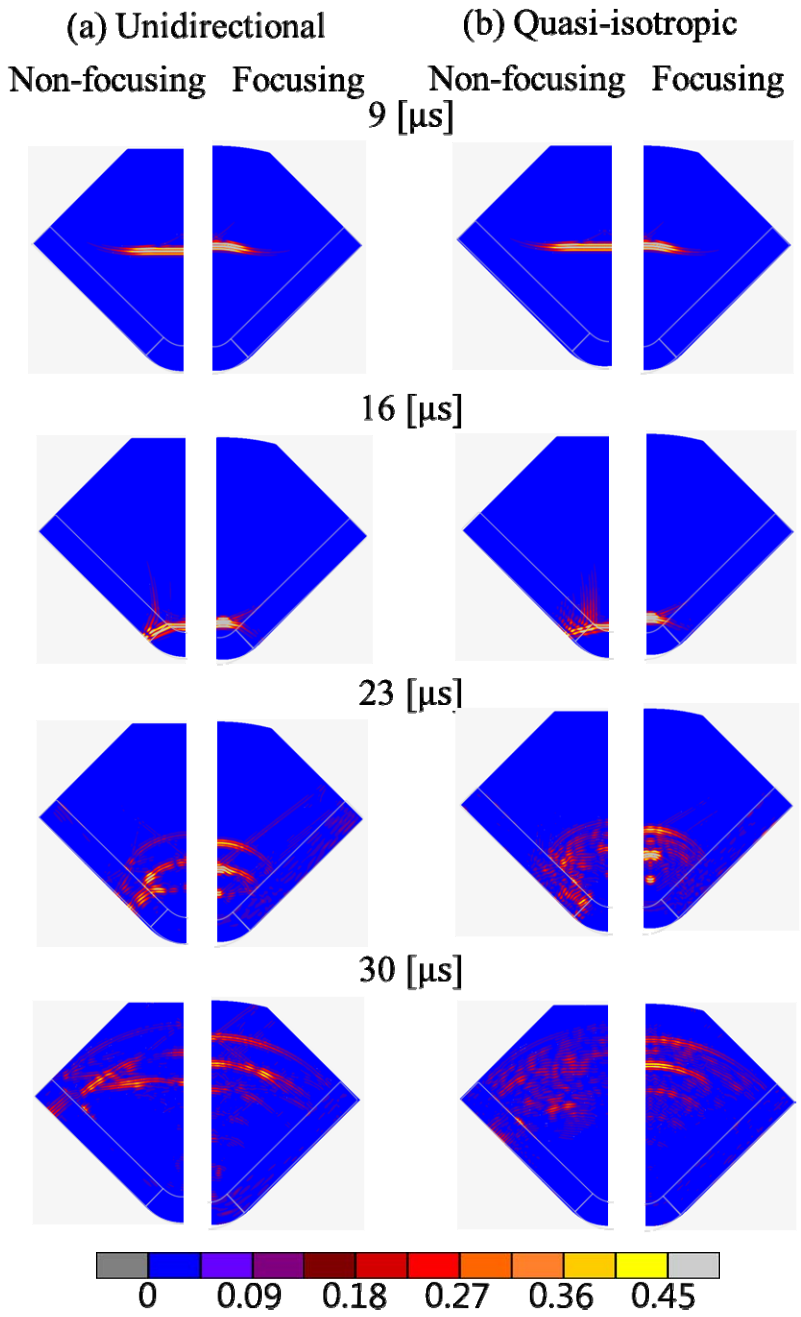

Fig. 2 Snapshots of wave propagation in the case of non-focusing and focusing of incident waves for (a) unidirectional and (b) quasi-isotropic laminates

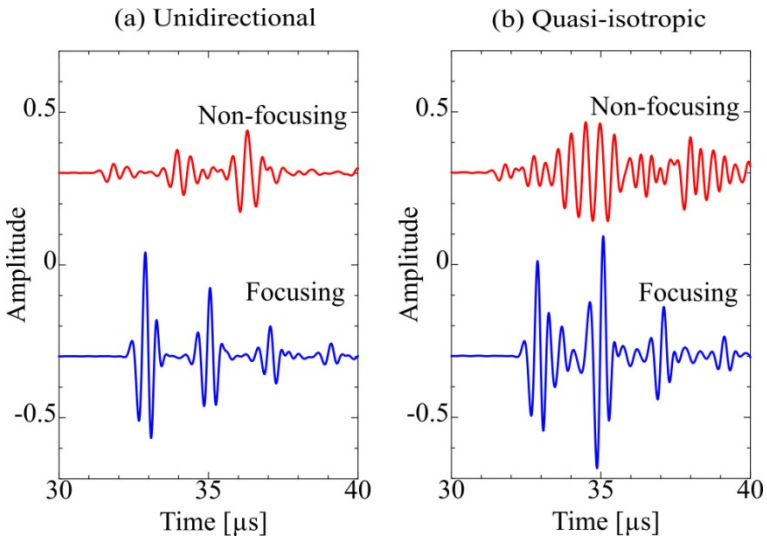

Fig. 3 Computed reflection waveforms in the case of non-focusing and focusing of incident waves for (a) unidirectional and (b) quasi-isotropic laminates

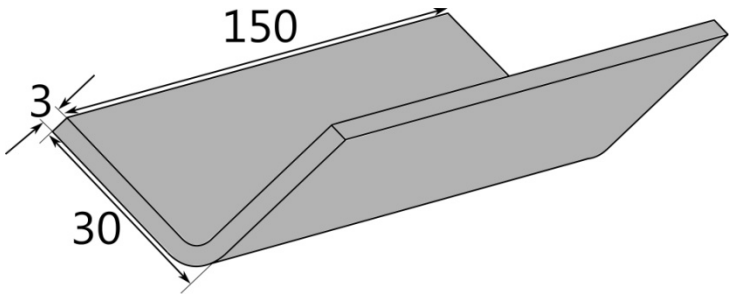

Fig. 4 Dimensions of the CFRP corner specimen

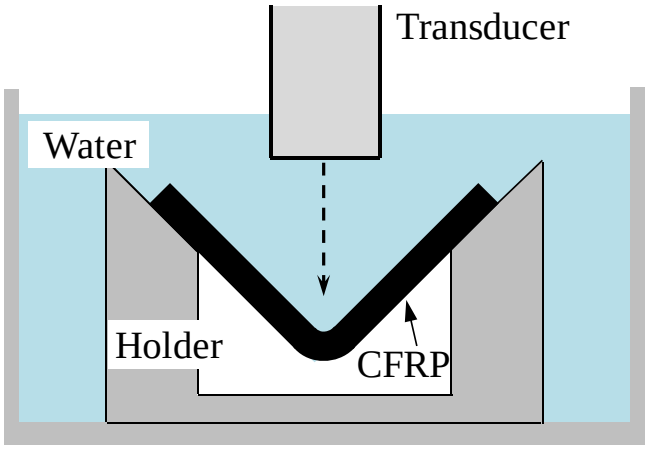

Fig. 5 Schematic illustration of the specimen arrangement in the reflection measurement

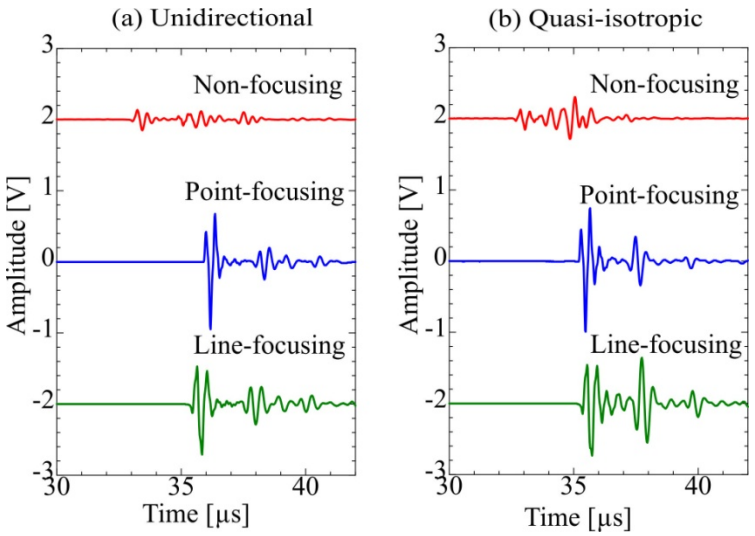

Fig. 6 Measured reflection waveforms obtained with non-focusing and focusing transducers for (a) unidirectional and (b) quasi-isotropic laminates

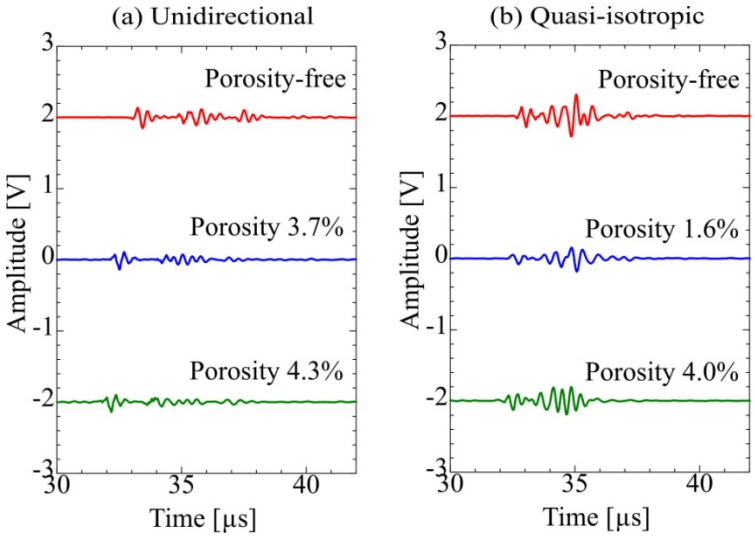

Fig. 7 Measured reflection waveforms obtained with the non-focusing transducer for (a) unidirectional and (b) quasi-isotropic laminates with different porosity contents

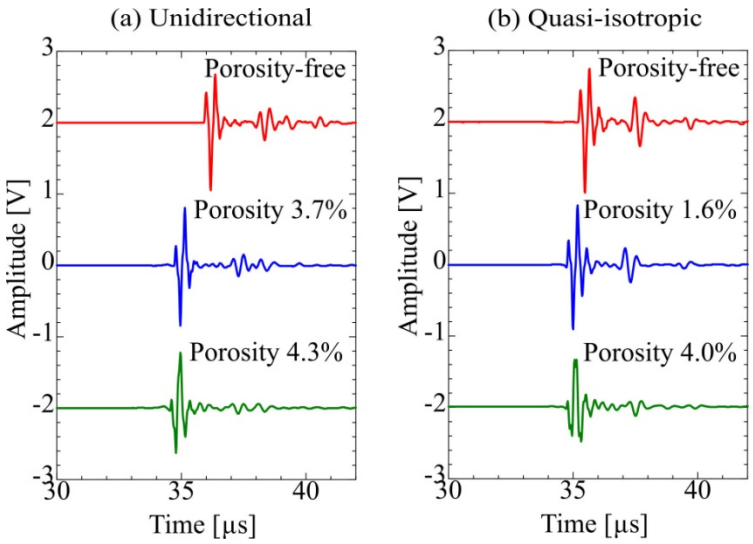

Fig. 8 Measured reflection waveforms obtained with the point-focusing transducer for (a) unidirectional and (b) quasi-isotropic laminates with different porosity contents

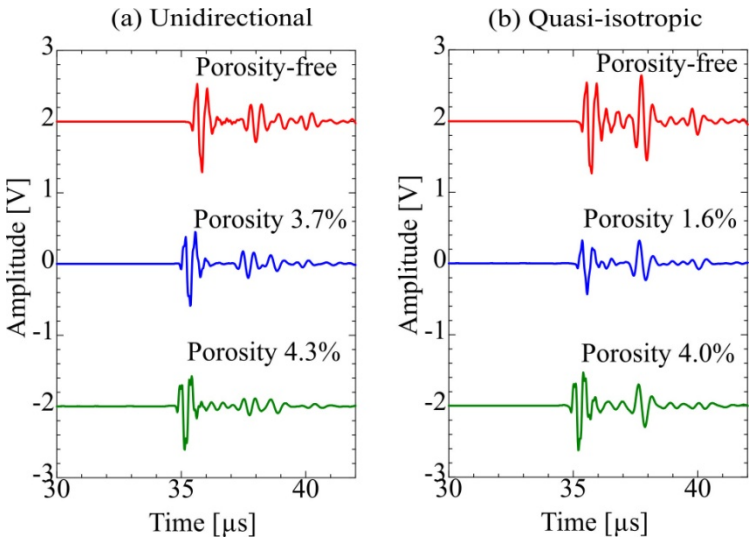

Fig. 9 Measured reflection waveforms obtained with the line-focusing transducer for (a) unidirectional and (b) quasi-isotropic laminates with different porosity contents

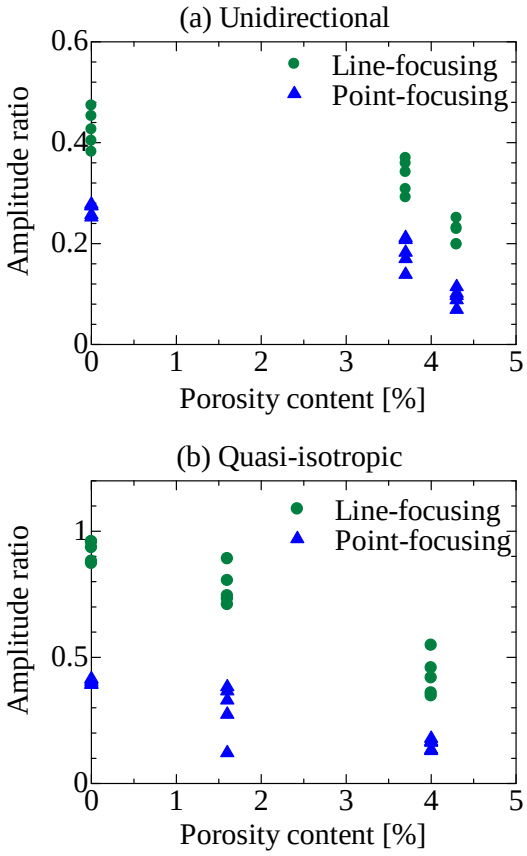

Fig. 10 Amplitude ratio of surface and bottom echoes with respect to the porosity content for (a) unidirectional and (b) quasi-isotropic laminates